RESEARCH ARTICLE

NANO · MICRO small
www.small-journal.com

Reaction with Water Vapor Defines Surface Reconstruction and Membranolytic Activity of Quartz Milled in Different Molecular Environments

*Chiara Bellomo, Valeria Lagostina, Cristina Pavan, Maria Cristina Paganini, and Francesco Turci**

Industrial processing of quartz (SiO_2) and quartz-containing materials produces toxic dust. Fracturing quartz crystals opens the Si–O bond and produces highly reactive surface species which mainly react with molecules like water and oxygen. This surface-reconstruction process forms silanol (Si–OH) on the quartz surface, which can damage biological membranes under specific configurations. To comprehend the impact of the quartz surface restructuring on membranolytic activity, the formation and reactivity of quartz radicals produced in four distinct molecular environments with electron paramagnetic resonance (EPR) spectroscopy are evaluated and their membranolytic activity is measured through in vitro hemolysis test. The four molecular environments are formulated with and without molecular water vapor and oxygen ($\pm H_2O/\pm O_2$). The absence of water favored the formation of surface radical species. In water-rich environments, diamagnetic species prevailed due to radical recombination. Quartz milled in $-H_2O/\pm O_2$ acquired membranolytic activity when exposed to water vapor, unlike quartz milled in $+H_2O/\pm O_2$. After being stabilized by reaction with water vapor, the membranolytic activity of quartz is maintained over time. It is demonstrated that the type and the reactivity of radical sites on quartz are modulated by the outer molecular environment, ultimately determining the biological activity of milled quartz dust.

1. Introduction

Occupational exposure to respirable crystalline silica (RCS), mainly in the form of α-quartz, is related to the risk of developing silicosis, lung cancer, and autoimmune diseases.[1] Silicosis still represents a major occupational issue worldwide.[2] The variable toxic effects of RCS have been related to the surface chemical characteristics of the different quartz sources[3] and the comminution of quartz crystals was reported to generate quartz dust with a greater toxic activity.[4] Mechanical comminution, which occurs in mining, milling, sandblasting, polishing, and cutting, generates new fractured surfaces in quartz-containing materials.[5] Due to the peculiar (and still debated) electronic nature and moderate anisotropy of the Si–O bond in the trigonal system of silica $[SiO_4]^{4-}$ tetrahedra,[6] quartz fracturing does not proceed along preferential crystallographic planes, but the characteristic conchoidal fractures are formed.[7] The atoms at the newly formed surfaces are exposed to the reactive molecular environment, made of oxygen and water vapor, and undergo chemical transformations and topological rearrangements.[8] During fracturing, highly reactive species on the newly formed quartz surfaces rapidly recombine in more stable arrangements during a "surface reconstruction" process. Several surface features are generated on fractured quartz particles, and some of them have been proposed as key determinants in inducing cell membrane damage and triggering

C. Bellomo, V. Lagostina, C. Pavan, M. C. Paganini, F. Turci
Department of Chemistry
Università degli Studi di Torino
Torino 10125, Italy
E-mail: francesco.turci@unito.it

The ORCID identification number(s) for the author(s) of this article can be found under https://doi.org/10.1002/smll.202308369

DOI: 10.1002/smll.202308369

C. Bellomo, C. Pavan, F. Turci
"G. Scansetti" Interdepartmental Center for Studies on Asbestos Other Toxic Particulates
Università degli Studi di Torino
Torino 10125, Italy

C. Pavan
Louvain Center for Toxicology
Applied Pharmacology
Université catholique de Louvain
Brussels 1200, Belgium

M. C. Paganini
NIS interdepartmental Center for Nanomaterials for Industry and Sustainability
Università degli Studi di Torino
Torino 10125, Italy

inflammation, which is the early pathogenic event underlying silicosis and lung cancer.[9] Among these surface features,[3b] a unique group of silanols (≡Si–OH), termed the "nearly-free silanols (NFS)", has been linked to the ability of quartz to interact with membrane phospholipids and initiate inflammatory responses.[10] NFS were not found on synthetic, defect-free quartz crystals, but formed immediately after quartz fracturing.[11]

The positive correlation between NFS induced during quartz milling and cell membrane damage represents a tremendous advance in the molecular understanding of the mechanisms of silica toxicity. However, the chemical sites generated during milling and the environmental parameters and kinetics that regulate the reconstruction of quartz surface, that is, the evolution of defective species towards more stable silanol groups, remain largely unexplored. During quartz fracturing, both radicals and charged species are formed, depending on the homolytic or heterolytic cleavage of the Si–O bond. Silica unsaturated surface sites have been studied with ab initio cluster calculation, photoluminescence, and electron paramagnetic resonance (EPR) spectroscopy.[12] While photoluminescence is the main technique of characterization of defects of γ-irradiated quartz,[13] EPR spectroscopy is the most commonly adopted technique to investigate ground quartz. The radical species generated by homolytic cleavage of the Si–O bond include the silyl ($Si^{\bullet}$), siloxyl ($Si{-}O^{\bullet}$), and other paramagnetic species[14] that can often be detected by EPR spectroscopy.[7b,15] When heterolytic cleavage occurs, silyl (Si^{+}) and siloxyl ($Si{-}O^{-}$) ions are mainly formed.[14] Several computational studies investigated the stability of radicals and ions but results are not conclusive. Cluster calculations suggested the lower stability of the charge separation generated by the heterolytic breakage with respect to the homolytic one.[16] Conversely, spin-polarized and spin-paired calculations indicate a surface energy difference between the two active sites of less than 2%. However, these calculations do not take into account intersite electrostatic interactions.[17] Additionally, several radical species may be generated when gas/vapor molecules that are present in the milling environment react with silica unsaturated sites that occur at the surface of fractured quartz. For instance, the presence of O_2 is held responsible for the generation of peroxyl and surface-bound superoxide radicals (≡$SiOO^{\bullet}$ and ≡Si^{+} $O_2^{-\bullet}$, respectively).[15b,18] In general, molecules in the outer environment modulate the chemistry of the newly formed surface and ultimately determine the surface reconstruction process of quartz.

The distinct reactivity of electronic defects in fractured quartz has drawn the attention of scientists for years, and these centers were investigated either for their possible role in triggering cytotoxicity and pathogenicity,[19] for catalysis in polymeric chain reactions,[20] for mineralogic characterization,[18] industrial engineering of materials[21] and in prebiotic chemistry as a catalyst for amide bond formation.[22] Recently, surface radical species that are generated during quartz fracturing have been proposed as an abiotic source of oxidants in the anaerobic Archean era. Being the most common mineral on Earth, quartz surface radicals reacted with surrounding water to produce H_2O_2 and O_2 and forced ancestral cyanobacteria to develop oxygenic photosynthesis.[23] The molecular understanding of the reactivity of fractured quartz is currently yielding remarkable cross-disciplinary advances, from the general mechanism of particle toxicology[10a,24] to some fundamental questions about the origin of life on Earth.[25]

In this work, we clarify the influence of the molecular environment that assists the surface reconstruction process of quartz, during and after mechanical fracturing. A pure quartz specimen was ball milled in four different molecular environments that combined the absence and presence of molecular water and oxygen, specifically $-H_2O/-O_2$, $-H_2O/+O_2$, $+H_2O/-O_2$, $+H_2O/+O_2$. The type and the relative abundance of radicals that were generated during the surface reconstruction process have been monitored by means of solid-state EPR spectroscopy. The specific reactivity and the stability over time of the generated radicals were assessed with several probe molecules (H_2O, O_2, CO) and thermal treatments up to 673 K. Finally, the reconstructed surfaces were tested for their potential to destabilize cell membrane by quantifying their lytic activity towards red blood cells (RBC).

This work represents the first attempt to systematically explore how the variation in the molecular environment during and after quartz fracturing affects the membranolytic activity of the quartz surface. The results represent an advance in the ongoing debate about the role of surface molecular moieties responsible for silica interaction with biological molecules and cellular membranes.

2. Results and Discussion

2.1. Molecular Environment Affects the Radical Profile of Milled Quartz

A general scheme of the species that can be generated during the surface reconstruction of milled quartz is reported in **Figure 1**. The contribution of the different molecular environments is highlighted, and seven reaction paths are depicted. The scheme is consistent with the previous literature and is intended to guide the reader in the analysis of the effect of the different environments, rather than proposing an actual mechanistic explanation about the formation of surface moieties on quartz. Upon formation of a silyl radical ($Si^{\bullet}$) from the Si–O homolytic cleavage (reaction 1), a siloxyl radical ($SiO^{\bullet}$) is expected to form. Silyl and siloxyl radicals may react with oxygen or water and convert into peroxyl radicals or silanol moieties (reactions 5 and 6, respectively). Two vicinal siloxyl radicals may also react and yield a peroxyl and a silyl radical (reaction 7). Heterolytic cleavage of the Si–O bond yields charged species, that is, silyl cation and siloxyl anion (reaction 2), which upon reaction with water or oxygen may form a surface-bound superoxide radical (reaction 3) or silanols (reaction 4). Among these species, silyl, peroxyl, and superoxide can be detected by EPR spectroscopy, while $SiO^{\bullet}$ is EPR silent because of the degeneracy of the ground state, which implies a too fast relaxation rate for the detection of the signal.[13a,26]

To investigate the different routes of surface reconstruction of quartz, a pure mineral quartz specimen (Figure S1A—D, Supporting Information) was ball milled in four different controlled molecular environments summarized in **Table 1** (see Supporting Information for details).

Quartz was milled in a planetary ball miller to a micrometric size that is compatible with respirable crystalline silica (RCS) dust. The peculiar morphology of fractured quartz crystals was observed and the surface area was found to be

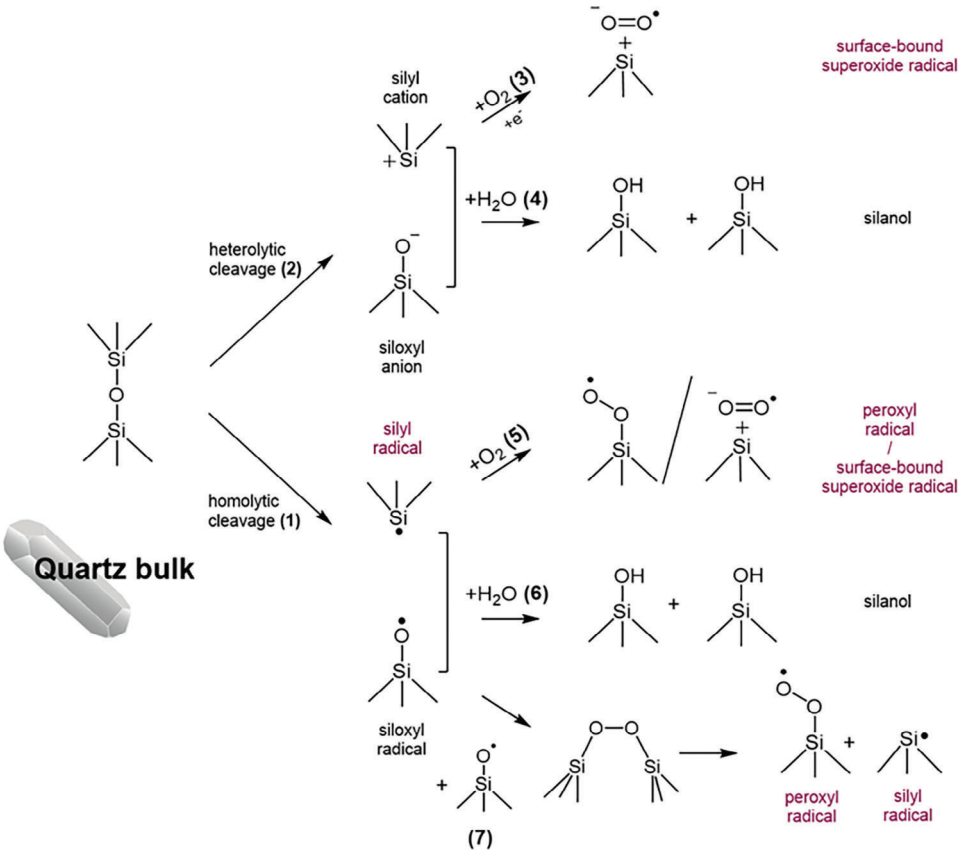

Figure 1. Schematic representation of the main reactions that might occur during the breakage of the Si–O bond in silica.[15b,23a,27] The species detectable with EPR spectroscopy are highlighted in red.

compatible with reference materials (Figure S1B,C, Supporting Information).[10a,11] Microstructural analysis and particle analysis distribution were performed on the four milled quartzes (Table S1 and Figure S1b, Supporting Information) and no significant changes were observed due to the different milling environments.

Following milling, any possible contamination was prevented by manipulating the milled quartz in a glove box ($pO_2 < 0.5$ ppm, $pH_2O < 0.5$ ppm) and storing the samples in sealed reservoirs. EPR spectra of milled quartz were acquired 24 h after milling (**Figure 2A**). The spectrum of quartz before milling (Figure 2A, non-milled) showed a negligible presence of EPR-active species. After milling, radicals were detected on all quartz samples, albeit to a very different extent. Under the most inert environment ($-H_2O/-O_2$), the EPR spectrum is dominated by the silyl radical ($Si^{\bullet}$). This species is often reported in the literature as the E' center.[15a] The silyl radical is generated by the homolytic opening of the Si–O bond or by the cleavage of a peroxide silanol bridge Si–O–O–Si, which may form by the condensation of two vicinal siloxyl radicals (Figure 1, Reactions (1) and (7)). Structurally, the silyl radical can be represented by a Si atom with a dangling bond located in a sp^3-like orbital. The signal has a nearly axial geometry dominated by the perpendicular component at $g_{\perp} = 2.0000$, which results from the two virtually coincident g_x and g_y tensors. The $g_{//}$ component of the signal, which is convoluted in the $g_{\perp}$ signal, is not visible at the available spectral resolution.[15a,26]

Other two EPR radical species could be observed in the spectrum of $-H_2O/-O_2$ quartz and were assigned to the peroxyl radical ($SiOO^{\bullet}$) and to the surface-bound superoxide radical ($Si^{+}O_2^{-\bullet}$). The spectral assignments were confirmed by

Table 1. Chemical characteristics of the four controlled molecular environments in which quartz was milled.

Sample	Milling environment	H_2O	O_2
$-H_2O/-O_2$	Argon ($O_2 < 0.5$ ppm, $H_2O < 0.5$ ppm)	NO	NO
$-H_2O/+O_2$	N_2 and O_2 mix (79–21%) + (H_2O, RH% = 0%[a])	NO	YES
$+H_2O/-O_2$	Argon + H_2O (RH% = 100%)	YES	NO
$+H_2O/+O_2$	Air [N_2 and O_2 mix (79–21%) + H_2O (RH% = 30–40%)]	YES	YES

[a] RH% = relative humidity at 25 °C.

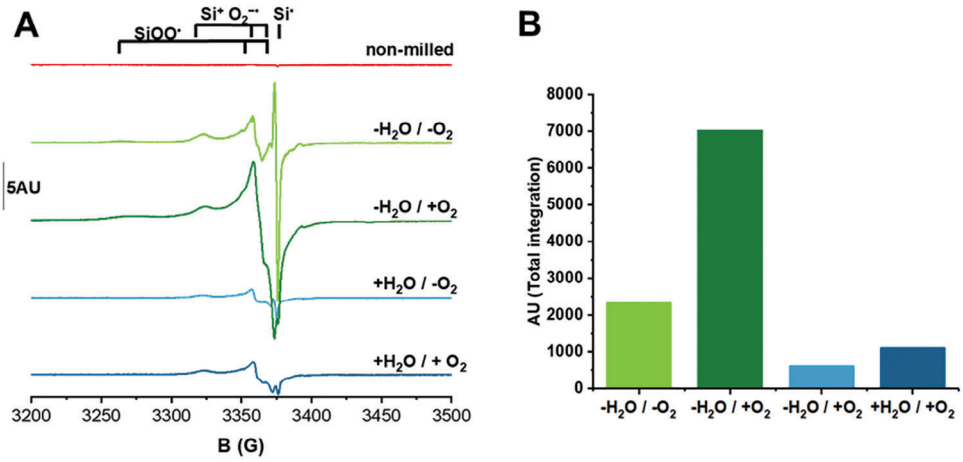

Figure 2. Effect of the molecular environment on the radical species generated during ball milling of quartz. A) EPR spectra of the quartz milled in the four different milling environments, recorded at 77 K and compared to the EPR spectrum of the non-milled quartz. Signals from three radical species are assigned to silyl ($Si^{\bullet}$, $g_x = 2.0000$, $g_y = 2.0004$, and $g_z = 2.0013$), peroxyl ($SiOO^{\bullet}$, $g_x = 2.0025$, $g_y = 2.0145$, and $g_z = 2.0668$), and surface-bound superoxide ($Si^{+}O_2^{-\bullet}$, $g_x = 2.0018$, $g_y = 2.0090$, and $g_z = 2.0325$) radicals.[15b,23a] All spectra were recorded at microwave power (MW) = 0.3 mW, which allowed us to clearly observe all three species (see the study of the attenuation frequencies on all the four milled quartzes reported in Figure S2, Supporting Information). B) Semi-quantitative comparison of the number of radical centers formed in the four milling environments, obtained by double integration of the experimental spectra. Signals were normalized according to the weight of the sample in the EPR cell.

simulating the EPR spectra (**Table 2** and Figure S3, Supporting Information). The peroxyl radical is strongly anisotropic in nature and exhibits the characteristic $g_z = 2.06–2.07$ ($g_z = 2.0668$, in this work). The unpaired electron occupies a 2p orbital of the oxygen atom, which is geometrically perpendicular to the projection plane of the silica surface.[29] In an oxygen-rich environment, the generation of peroxide species in quartz involves the reaction of the silyl ($Si^{\bullet}$) radical with molecular oxygen (Figure 1, Reaction (5)).[7b,21b] The reaction is commonly observed during thermal annealing of SiO_2 at $T > 400$ °C, and followed by the characteristic increase of peroxyl radical EPR signal intensity.[30] In our experimental settings, the activation energy for the formation of peroxyl radical could be provided by the mechanochemical process, but the oxygen-free environment requires that oxygen is provided by a structural rearrangement of the quartz lattice during ball milling. Under mechanic deformation, the generation of peroxyl bridges (≡Si–O–O–Si≡) may follow the distortion of the crystal lattice of quartz. The Si–O homolytic cleavage of this species yields a peroxyl and a silyl radical (Figure 1, Reaction (7)).[27,31] The superoxide radical is generally formed by the reduction of molecular oxygen from an electron donor center and the subsequent stabilization of the superoxide anion by a silyl cation ($\equiv Si^{+}$), at the quartz surface (Figure 1, Reaction (3)). This partially reduced radical species originates an intermolecular adduct, with the unpaired electron located in a π^* antibonding orbital. The generation of superoxide radicals via the reduction of the molecular oxygen in our oxygen-free environment is necessarily limited, as proved by the low intensity of the EPR signal of this species. Nonetheless, the formation of a few superoxide radicals could be explained by the occurrence of traces of residual oxygen, which could be available for reduction during milling (Figure 1, Reaction (5)).[32] The role of oxygen was experimentally highlighted by observing that a 5-fold increase in the milling time produced a dramatic increase in the amount of silyl and peroxyl but not superoxide radical (Figure S4, Supporting Information).

Table 2. Simulated values of the *g*-tensor for the silyl radical, the peroxyl radical, and the surface-bound superoxide radical reported in this work and compared with the corresponding literature reference.

	g_x	g_y	g_z	Ref.
$Si^{\bullet}$	2.0000 ($g_{\perp}$)	2.0004 ($g_{\perp}$)	2.0013 ($g_{//}$)	This work
$SiOO^{\bullet}$	2.0025	2.0145	2.0668	
$Si^{+}O_2^{-\bullet}$	2.0018	2.0090	2.0325	
$Si^{\bullet}$	2.0003	2.0007	2.0017	[15a]
	2.0000	2.0000	2.0020	[26]
$SiOO^{\bullet}$	2.002	2.007	2.056	[15b]
	2.0025	2.0082	2.0719	[28]
$Si^{+}O_2^{-\bullet}$	2.002	2.010	2.04-2.03	[15b]
	2.002	2.010	2.044	[23a]

When molecular oxygen was present in the milling environment (Figure 2, spectrum $–H_2O/+O_2$), a dramatic change in the EPR signal shape and intensity was observed, with respect to the water- and oxygen-free environments. Silyl, peroxyl, and surface-bound superoxide radicals were still observed at the quartz surface, but the signals of the latter two species were largely more intense than the signal of silyl. The presence of molecular oxygen in the milling environment favored the formation of oxygenated radicals. The strong intensity of the EPR spectrum suggests that molecular oxygen reacts with surface active sites generated by crystal fracturing, by creating oxygen-centered radicals (Figure 1, Reactions (3) and (5)).

When water vapor was present in the milling environment (Figure 2, spectra $+H_2O/–O_2$ and $+H_2O/+O_2$), the intensity of the radical profiles of milled quartz was significantly lower than the profiles of quartz milled in water-free environments. These data proved that water vapor readily interacts with the radical sites that occur on quartz surfaces and converts them into

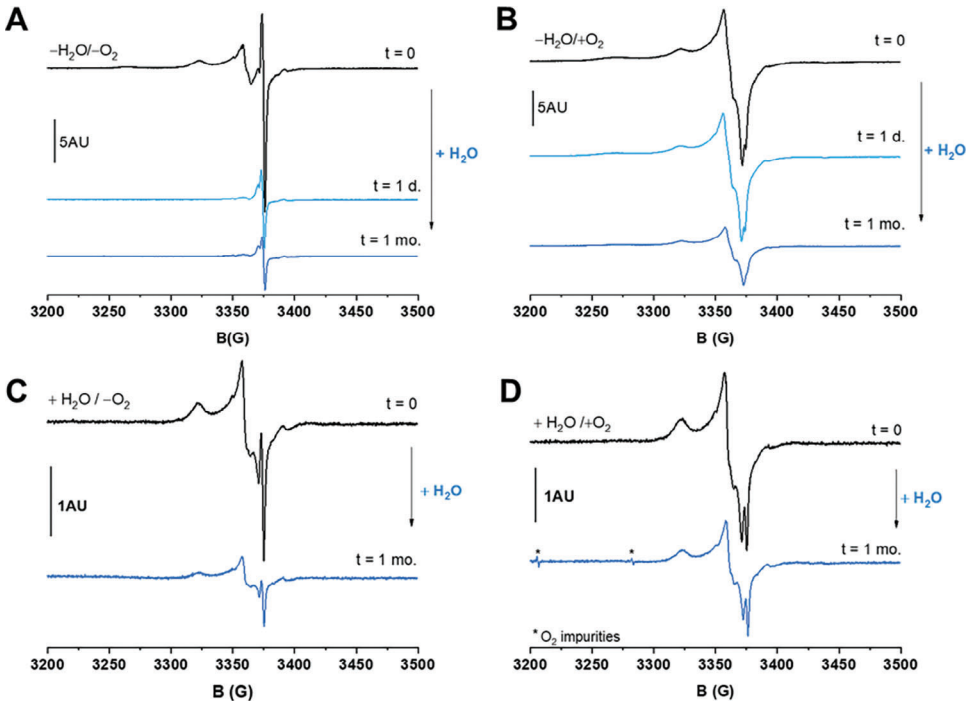

Figure 3. EPR signals of quartz milled in the four molecular environments and exposed to water vapor at different time points. Spectra of quartz milled in A) $-H_2O/-O_2$, B) $-H_2O/+O_2$, C) $+H_2O/-O_2$, and D) $+H_2O/+O_2$ before ($t = 0$) and after exposure to 25 mbar of H_2O vapor for $t = 1$ day and 1 month are recorded at 77 K after degassing the EPR cell.

nonparamagnetic species, likely silanols (Figure 1, Reactions (4) and (6)). Transient radical species ($^{\bullet}OH$ and $H_3O^{\bullet}$) are generally formed during these reactions and rapidly recombine to generate easily degassed molecular species (H_2O, H_2O_2).[23a,c,d,25] Those transient species have been recently investigated and might have a role in the formation of the more stable radicals detected in this work.[33]

The double-integrated values of the EPR spectra of quartz that was milled in the four environments are reported in Figure 2B. The integration describes semi-quantitatively the overall amount of paramagnetic species that were detected on milled quartz. Signal intensities were directly comparable because experiments were performed on equal masses of samples. When oxygen was present in the water-free milling environment ($-H_2O/+O_2$), a dramatic increase of total surface radicals was recorded with respect to quartz milled in an inert environment ($-H_2O/-O_2$). This increase is compatible with the largely increased amount of $Si^{+}O_2^{-\bullet}$ and $SiOO^{\bullet}$ detected on $-H_2O/+O_2$ with respect to an oxygen-free environment. Consistently with qualitative observations discussed above, the presence of water strongly reduced the amount of radical species also in the presence of oxygen ($+H_2O/\pm O_2$).

Overall, our data support a molecular mechanism of radical generation that yields mainly E' centers (and the EPR-silent $SiO^{\bullet}$) when milling is performed in an oxygen- and water-free environment. The presence of oxygen dramatically increased the amount of radicals, especially favoring the generation of oxygen-centered radicals. The formation of oxygen-centered radicals also supports the existence of the EPR-silent $SiO^{\bullet}$, which may concur with the formation of $SiOO^{\bullet}$ through the reactions reported in Figure 1, Reactions (6) and (7). Water vapor, also in combination with oxygen, strongly reduced the overall amount of radical species by reacting with surface radicals and forming surface silanols (Figure 1, Reactions (4) and (6). The larger amount of radicals that were generated in water-free environments with respect to water-rich environments is consistent with an energetically favored homolytic cleavage of the Si–O bond in non-polar environments, such as Ar or O_2.

It is worth noting that the mechanical stress applied to quartz during milling was energetically identical for the four samples, as the four procedures only differ for the molecular composition of the milling environment. This implies that the large qualitative and quantitative differences observed in the radical species of the four-milled quartz are only due to the absence or presence of the two investigated molecules. In turn, this suggests that the vast majority of the radicals that are formed during the mechanochemical process are surface species.

2.2. Radicals on Milled Quartz Exhibit Site-Specific Reactivity

To further elucidate the specific reactivity of the surfaces obtained by milling quartz in the four different environments, the milled samples were in contact with saturated water pressure for up to 1 month. EPR signals of the radical species were recorded at 77 K and compared with those recorded for the freshly ground quartz reported in Figure 2A (**Figure 3**). The four $\pm H_2O/\pm O_2$ milled quartz samples were contacted with ≈25 mbar of water vapor. On the $-H_2O/-O_2$ quartz surface, water molecules selectively reacted with superoxide and peroxyl species, and a complete suppression

Table 3. Percentage of decrease of the EPR spectra intensity after exposure to water vapor, with respect to the intensity of the $t = 0$ spectra. Data were calculated by double integrating spectra in Figure 3.

	$-H_2O/-O_2$	$-H_2O/+O_2$	$+H_2O/-O_2$	$+H_2O/+O_2$
1 day	90%	19%	n.a.	n.a.
1 month	94%	60%	82%	54%

of their signals was observed after 1 day (Figure 3A). The reaction of oxygenated radicals with water is irreversible, as proved by the shape of the spectrum, which is not restored to pristine shape when water is outgassed from the EPR cell. Quantitative data, reported in **Table 3**, highlights that ≈90% of the radical species on $-H_2O/-O_2$ quartz irreversibly react with water vapor already 1 day after exposure. The reaction between water and silyl and siloxyl radicals (Figure 1, Reaction (6)) involves the generation of surface silanols.

The observed process of quartz surface reconstruction with water is in good agreement with computational studies, which observed that a cleaved surface of quartz is able to exothermally react with water vapor.[14,34] After 1 day of exposure to water, $-H_2O/-O_2$ quartz surface exhibited a strong reduction, but not a complete suppression, of the silyl radical intensity, with respect to the pristine quartz non-exposed to water vapor. This behavior, further highlighted by the spectrum at $t = 1$ month (Figure 3A), suggests that the E' center exhibits a lower reactivity than oxygen-centered radicals, likely due to a lower accessibility with respect to the other radical species. This is consistent with previous findings on the evolution of the radical profile of quartz samples that were analyzed months or years after milling and were characterized by the main presence of E' centers.[11,35] Possibly, a certain amount of silyl radicals in milled quartz is hosted in subsurface layers and in the grain borders of the material.[15b,35] Those subsurface E' centers might not be directly accessible to water molecules and their arrangement implies that the kinetics of the conjugation with water is controlled by the negligible diffusion coefficient of molecular water in quartz. Conversely, peroxyl and superoxide species fully react with water vapor, highlighting the strong surface nature of these active species. This aspect is relevant to the formation of surface silanols. He and co-workers[23a,c] recently proposed that the reaction between surface $SiOO^{\bullet}$ and $Si^{+}O_2^{-\bullet}$ may indeed also yield silanol.

$$\equiv SiOO^{\cdot} + H_2O \rightarrow \equiv SiOH + HO_2^{\cdot} \quad (1)$$

$$\equiv Si + O_2^{-\cdot} + H_2O \rightarrow \equiv SiOH + HO_2^{\cdot} \quad (2)$$

In both reactions, (Equation (1) and (2)) hydroperoxide radical ($HO_2^{\bullet}$) may recombine and yield H_2O_2 and O_2.[25] The specific reactivity of water with surface radicals was further highlighted by comparing the spectrum of $-H_2O/-O_2$ exposed to water vapor for $t = 1$ month with the spectrum of $-H_2O/-O_2$ stored in a non-reactive environment (Ar) for the same amount of time. The radical population of this latter sample was reduced only by 30% (Figure S5, Supporting Information), while the former sample was reduced by 94% (Table 3).

The exposure to water vapor was performed on the $-H_2O/+O_2$ sample. In this case, the rapid and selective reactivity of peroxyl and superoxide with water was not observed. In fact, the signal shape and intensity remained almost unchanged after 1 day, with an overall reduction of only 19% of the radicals present compared to the original sample (Figure 3B and Table 3). This indicates that the oxygenated radicals generated in the $-H_2O/+O_2$ environment are more stable than the same species in the $-H_2O/-O_2$ milled quartz. When the $-H_2O/+O_2$ quartz was exposed to water vapor for 1 month, the reduction in the total EPR signal intensity (60% in Table 3) was not accompanied by a selective reduction of the oxygenated species but rather produced a progressive decrease in the total intensity of the radical signals over time. This non-specific reduction in signal intensity also occurred, although to a different extent, in the two other milled quartz samples ($+H_2O/\pm O_2$, Figure 3C,D) that were exposed to water vapor for 1 month. In both cases, the decrease of the EPR signal was not accompanied by a selective reduction in the oxygenated species but rather produced a progressive decrease in the overall radical species over time. However, the reduction in the total EPR signal intensity was much greater for the quartz milled in the oxygen-free environment than for the quartz milled in the oxygen environment. The former showed a significant decrease in EPR signal (82%), while the latter showed only a 54% decrease in EPR signal. This indicates that there is a distinct stabilization of the radicals produced during milling that is reliant on the molecular environments present during the milling process. Our data support the hypothesis that the radical species that are formed in the four molecular environments are similarly located at the quartz surface. Nevertheless, their reactivity appears to be specifically modulated by the molecular environment in which each different surface was reconstructed. Specifically, the absence of water and oxygen during milling generates the most reactive surfaces, while the presence of oxygen promotes the formation of more stable surfaces. A detailed investigation of this aspect was beyond the purpose of this work. However, it can be speculated that molecular oxygen promotes a partial surface reconstruction which is hindered in oxygen-free milling environments.

To further probe the reactivity of milled quartz surfaces, we exposed the $-H_2O/-O_2$ milled quartz to O_2 and CO probe molecules (Figure S6, Supporting Information). Exposure to molecular oxygen showed a totally reversible interaction with surface radicals. When added to the EPR cell, molecular oxygen ($pO_2 = 30$ mbar, $T = 77$ K) immediately suppressed the $SiOO^{\bullet}$ and $Si^{+}O_2^{-\bullet}$ signal, while the silyl radical remained largely unaltered by the interaction with O_2 absorbed on the surface. The pristine shape of the $-H_2O/-O_2$ EPR signal was completely restored upon outgassing, suggesting that: i) Peroxyl and superoxide radicals are superficial in nature, and ii) the interaction of quartz radicals with molecular oxygen is completely reversible. The different reactivity of oxygen and water is somehow expected and likely resides in the different polarizability of the two molecules. Furthermore, the reversible interaction with oxygen suggests that reactions 3, 5, and 7 (Figure 1) are unlikely to occur on these reconstructed surfaces. During milling, however, the combined presence of molecular oxygen and mechanochemically induced high-energy states favors the formation of oxygenated radicals. Exposure to molecular CO (pCO = 5 mbar, Figure S6, Supporting Information, panel B) and the thermal treatments in vacuum (Figure S7, Supporting Information) further highlighted the higher reactivity of the peroxyl radical with

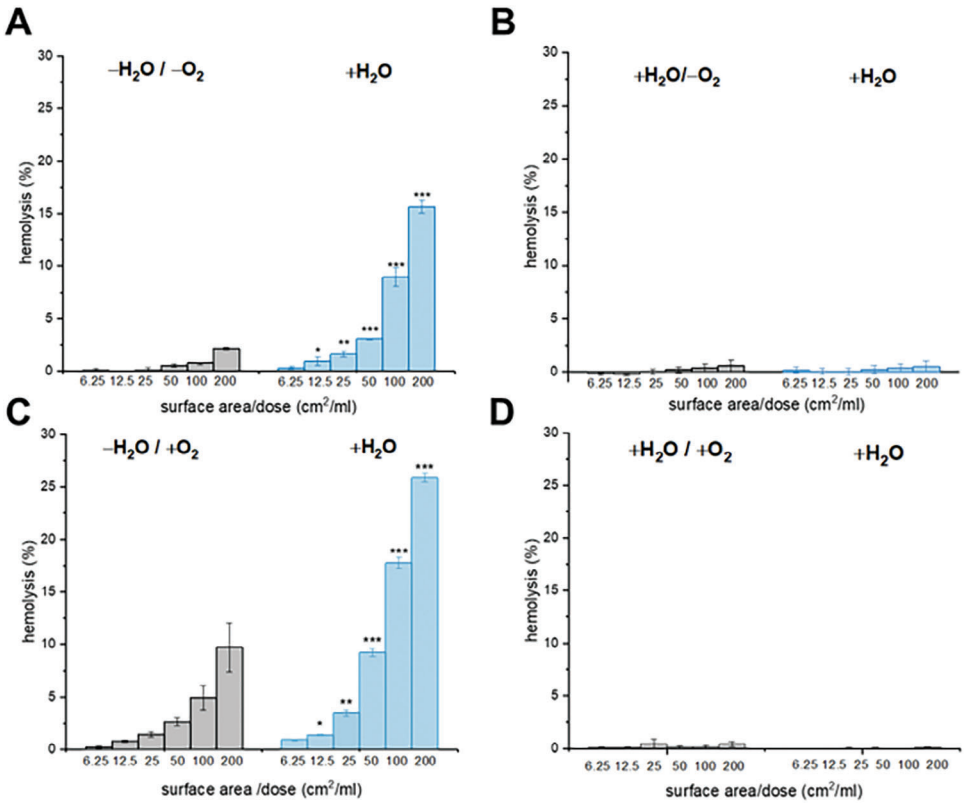

Figure 4. Membranolytic activity of the milled quartz in the four different environmental conditions before (grey bars) and after exposure to water vapor (blue bars). Values are means ± SD and are compared with a two-tailed Student's *t*-test; milled quartz before versus after exposure to water vapor at each dose: $*p < 0.05$, $**p < 0.01$, and $***p < 0.001$.

respect to the other radical species. The thermal treatments evidenced the specific stability of the three radical species. At low temperature (373 K) only the peroxyl radical signal was affected (Figure S7A, Supporting Information). At higher temperatures (673 K), all radical species were annealed, except for a small amount of E' centers. Since the experiments were conducted in vacuum, the progressive annealing of defects in quarts can be attributed to the recombination of radicals into more stable structures, likely siloxanes.[24b] The reactivity and the EPR spectra of thermally annealed quartz strongly suggest that the paramagnetic defects induced by milling have the following stability: $SiOO^{\bullet} < Si^{+}O_2^{-\bullet} < Si^{\bullet}$.

2.3. Membranolytic Activity of Milled Quartz Surface is Modulated by the Milling Environment

EPR spectroscopy revealed that the external environment is able to modulate the reactivity and the relative abundance of radical sites on the surface of milled quartz. Upon surface reconstruction, such modulations likely translate into different silanol populations which in turn might exhibit specific membranolytic activities. It was recently shown that the membranolytic activity of quartz is directly linked with the occurrence and the specific arrangement of some silanol families at the quartz surface.[10a] Even if radical sites on the particle surface or particle-generated reactive oxygen species in solution (ROS, i.e., hydroxyl, superoxide, and peroxyl radicals)[3b] may contribute to the oxidative stress in the lung,[2b] the molecular initiating event (MIE) of quartz inflammatory pathway (i.e., the membranolysis of the phagolysosome) is currently correlated with the occurrence of NFS on quartz surface. In fact, no correlation between ROS generation and membranolytic activity was often observed[3b,10a,36] but a large panel of silica and silica-based materials confirmed the central role of NFS in the establishment of specific interactions with zwitterionic phospholipids in cell membranes.[10b,37] To measure this interaction, we used non-internalizing cells (red blood cells, RBC) that limit the potential interaction with particles to the outer lipid bilayer of their cytoplasmatic membrane. RBC does not have a role in the inflammatory or fibrotic responses induced by quartz particles, but their membrane is a convenient model[38] and the hemolysis test is largely used to evaluate the pro-inflammatory activity of quartz dust.[24b,36] Furthermore, hemolytic activity is considered one of the best predictors of in vivo inflammation for metal oxide nanoparticles.[39] To investigate how surface reconstruction impacts the membranolytic activity of the quartz, the quartz samples that were ball milled in the four molecular environments ($\pm H_2O/\pm O_2$) were contacted with RBC and hemolytic activity was measured (**Figure 4**). Samples ball milled in water-free environments exhibited a low ($-H_2O/-O_2$) or moderate ($-H_2O/+O_2$) membranolytic activity (Figure 4, panels A and C, grey bars). The observed membranolytic activity can reside in the specific reactivity of some surface sites of quartz with liquid water, in which the hemolysis test is carried out. The hemolytic activity

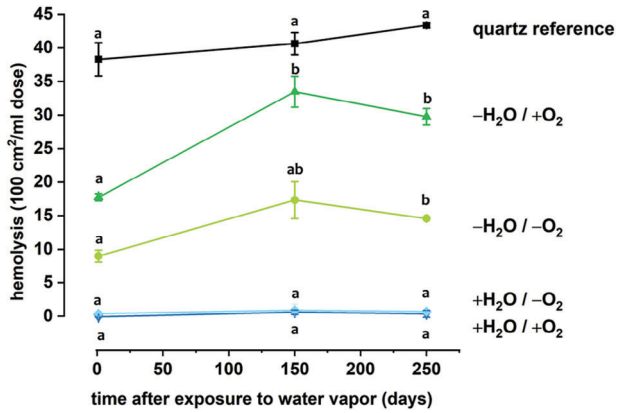

Figure 5. Membranolytic activity of the quartz (100 cm^2 ml^{-1}) milled in the four different environmental conditions ($t = 0$) and exposed to water vapor at different time points (1, 150, and 250 days). Industrial quartz was used as reference quartz because of its well-known membranolytic activity and measured at the same time points.[36,40] Values are means ± SD and values with different letters are significantly different ($p < 0.05$), as estimated by repeated measure one-way ANOVA with Tukey's post-hoc test.

of the quartz milled in the water-free environments dramatically increased as soon as they were exposed to water vapor (≈25 mbar) (Figure 4A,C, blue bars). Conversely, the samples milled in water-rich environments ($+H_2O/\pm O_2$) resulted in being totally inactive toward RBC membranes, with hemolysis percentages <1% also at the highest doses and their activity was still negligible after reaction with water vapor (Figure 4B,D). These data highlight that the exposure to water vapor, during and after milling, is the determinant for membranolytic quartz surfaces. Mechanistically, we could speculate that only quartz milled in a water-free environment exposes surface radical sites that can rapidly combine with water and yield specific silanol families, that in turn confer membranolytic activity to the particles. When quartz is milled in water-rich environments, such radical sites might not be present or be accessible to water vapor. Moreover, the physical state of water in the process seems to play a crucial role. In fact, we observed that the reactive surfaces of $-H_2O/\pm O_2$ quartz were dramatically altered by the reaction with vapor water but not with liquid water. This phase-specific reactivity of silica radicals towards water was recently reported by Xia and co-workers,[25] who observed a higher generation of ROS from the silica surface when the particles were exposed to water vapor rather than liquid water.

2.4. Aging Environment Alter the Membranolytic Activity of Milled Quartz

To further investigate the reactivity of milled quartz surfaces towards water vapor, we exposed the $\pm H_2O/\pm O_2$ quartz in water vapor (time up to 250 days, RH% = 100) and measured their membranolytic activity at the following time points: 1, 150, and 250 days (dose 100 cm^2 ml^{-1}). The kinetics showed that the membranolytic activity of $-H_2O/\pm O_2$ quartz exposed to water vapor was preserved with time up to 250 days (**Figure 5**, green lines). A significant increase in the hemolytic activity of the $-H_2O/+O_2$ and, to a lower extent, of the $-H_2O/-O_2$ quartz was observed after 150 days of incubation with water vapor. The membranolytic activity of the $+H_2O/\pm O_2$ quartz remained negligible for up to 250 days. These data suggest that fast and irreversible reactions take place between water vapor and surface radicals at quartz surface upon milling and that the surface species formed in the process are stable and responsible for the membranolytic activity of quartz. The presence/absence of oxygen ($-H_2O/\pm O_2$) also slightly differentiated the reactivity of quartz with water vapor, possibly due to the higher amount of radical species observed on $-H_2O/+O_2$, which reasonably also increased the membranolytic activity with time.

3. Conclusion

This work explored the effects on the surface reconstruction pathways and the membranolytic activity of four quartz samples obtained by combining the absence and presence of molecular water vapor and oxygen during milling. We observed that water- and oxygen-free environment mainly generates silyl surface radicals (E' centers). Oxygen-rich environment favors the peroxyl and surface-bound superoxide radicals, with respect to E' centers. Water-rich environment, on the contrary, reduces the number of electronic defects and converts them into diamagnetic species, likely surface silanols. The four environments yield surface radicals with specific reactivity towards molecular probes. Water-free environments ($-H_2O/\pm O_2$) generate quartz that is characterized by a strongly reactive surface and immediately interacts with water vapor. On the contrary, water-rich environments ($+H_2O/\pm O_2$) generate quartz that is characterized by negligible membranolytic activity, even after 250 days of exposure to water vapor. Mechanistically, E' centers, which largely dominate the surface of quartz milled in a water-free environment, might be responsible for the generation of the membranolytic silanol species, after reaction with vapor, but not liquid, water. This latter specific reactivity likely resides in the different activation energies of the $Si^{\bullet} + H_2O$ (vap) or H_2O (liq) reactions, as recently also observed by Xia and co-workers.[25]

4. Experimental Section

Materials: Ultrapure (UP) water (MilliQ, Merck) was purified through a sterile filter of 0.22 µm pore size before use. Gases used (Ar, O_2, dry air, CO) were purchased from SAPIO, Italy.

The pristine quartz used in all experiments was made up of centimetric crystals, it was mined in Madagascar and was highly pure.[3b]

Red blood cells from sheep blood were purchased from Thermo Fisher and purified prior to use.

All the other reagents were purchased from Sigma Aldrich (Merck) and used as received.

Ball Milling Procedure: Centimetric quartz crystals (≈10 g, "before milling" BM quartz) were preliminarily milled in a planetary ball mill (RETSCH S100) in an agate jar (volume: 45 ml) with one agate ball (diameter: 25 mm) for 3 h at 70 rpm. A fraction of this product (1.5 g, pre-milled PM quartz) was further milled for 1 h at 250 rpm (pause of 1 min every 20 min) in a planetary ball miller (FRITSCH P6) within a zirconia jar (45 ml) containing 41 g of zirconia balls (5 mm) in four different molecular environments ($-H_2O$ / $-O_2$; $-H_2O$ / $+O_2$; $+H_2O$ / $-O_2$; $+H_2O$ / $+O_2$ in Figure S1, Supporting Information).

Milling Environments: The pre-fractured quartz was milled in the following four molecular environments.

i. $-H_2O$ / $-O_2$ milling environment was obtained by working in an argon-filled glove box (MBraun LABstar glove box filled with pure 5.5 grade Ar, $O_2 < 0.5$ ppm, $H_2O < 0.5$ ppm);
ii. $-H_2O$ / $+O_2$ milling environment was obtained by working inside a glove bag filled with a N_2 and O_2 mix (79%–21%, "Aria zero" from SAPIO). To exclude water vapor from the glove bag five degassing cycles have been performed. The jar was charged with quartz inside the glove bag and sealed. After milling, the jar was opened again inside the glove bag.
iii. $+H_2O$ / $-O_2$ milling environment was artificially produced inside a glove bag filled with argon saturated with water vapor. Five cycles of degassing were carried out in order to exclude oxygen. The relative humidity (RH)% = 100% was measured with a portable hygrometer (ThermoPro TP157). The jar was loaded with quartz and reopened after milling in the same glove bag.
iv. $+H_2O$ / $+O_2$ milling environment corresponds to the external environment (79-21% mix of N_2 and O_2 and RH% = 30–40%).

Reactivity with Molecular Water Vapor: Quartz milled in the four environments was transferred in a sealed glass container and connected to a vacuum line (residual pressure 1×10^{-4} mbar). Saturated water vapor ($p_{sat} = \approx 25$ mbar) was expanded in the container and put in contact with quartz for different time points up to 8 months. At different time points, water-reacted samples were analyzed for radical species with solid-state EPR spectroscopy and membranolytic activity.

Solid State Electron Paramagnetic Resonance (SS-EPR) Spectroscopy: Twenty-four hours after milling ground quartz was inserted in an EPR cell in a controlled environment (glove box for $-H_2O$ / $-O_2$ and glove bags for $-H_2O$ / $+O_2$ and $+H_2O$ / $-O_2$), to avoid contamination from the external environment. The sealed EPR cell was attached to a conventional vacuum line (residual pressure: 1×10^{-4} mbar), outgassed, and inserted in the EPR spectrometer for the analysis. The analysis of the radical species was performed by SS-EPR spectroscopy at 77 K and at RT when required, by a Bruker CW-EMX spectrometer operating at an X-band (9.5 GHz). The spectra were recorded with the following instrument settings: i) Microwave power of 0.3 mW; ii) Modulation amplitude of 2G; iii) Center field at 3380 G, with a scan range of 400 G; and iv) 40 s, five scans. Spectra at different attenuation frequencies are reported in Figure S2, Supporting Information. Integrated values of EPR spectra were calculated using OriginPro 2023 (64-bit) ver. 10.0.0.154 Academic (OriginLab Corporation).

Simulations of the EPR Spectra: Spectra simulations were performed with EasySpin 6.0.0-dev.33 supported on MATLAB R2020b.[41]

Membranolytic Assay: Red blood cells (RBCs) were purified from sheep blood in Alsever's solution by centrifugation at 3200 × g for 2 min (Rotina 380R; Hettich, MA) and washed three times with 0.9% NaCl. RBCs were suspended in 10 mM PBS at the final concentration of 5% by volume. Sheep RBCs were used because they showed a sensitivity to silica very similar to that of human RBCs.[42] Particles were dispersed in 10 mM PBS and sonicated for 2 min in a bath just before testing. Serial dilutions of the starting particle dispersions (300 cm^2 ml^{-1}) were performed according to the final surface area doses used for experiments. Dispersions were distributed in quadruplicate in a transparent 96-well plate (150 µL per well), and the RBC suspension was then added (75 µL per well). Negative and positive controls consisted of 10 mM PBS and 0.1% Triton-X 100 in PBS, respectively. The plate was incubated on a plate shaker at 37 °C for 30 min and then centrifuged at 216 × g for 5 min. Supernatants were transferred to a new plate (75 µL per well), and the absorbance of the hemoglobin released was determined at 540 nm on a UV–vis spectrophotometer (Ensight, Perkin-Elmer, Waltham, MA) using the software Kaleido 2.0 (Perkin-Elmer).

Statistics: The data shown were means ± SD. Data were analyzed by two-tailed unpaired Student's *t*-test, or one-way analysis of variance (ANOVA) followed by Dunnett's post-hoc test, as appropriate. Differences with $p < 0.05$ were considered statistically significant. The GraphPad Prism 10.0.1 software (GraphPad Software, San Diego, CA) was used to perform statistical analysis.

Supporting Information

Supporting Information is available from the Wiley Online Library or from the author.

Acknowledgements

This study was supported by the European Association of Industrial Silica Producers (Brussels, Belgium) under the research contract "Surface Silanols as Key Descriptor of the Silica Hazard". The Authors acknowledge support from the Project CH4.0 under the MUR Program "Dipartimenti di Eccellenza 2023-2027" (CUP:D13C22003520001). The authors thank Prof. Bice Fubini, Prof. Piero Ugliengo, and Prof. Elio Giamello for enlightening discussion during the writing of the manuscript, and Dr. Maria Carmen Valsania for the SEM micrographs.

Conflict of Interest

The authors declare no conflict of interest.

Data Availability Statement

The data that support the findings of this study are available from the corresponding author upon reasonable request.

Keywords

membranolysis, quartz, silanols, surface radical, surface reconstruction

Received: September 21, 2023
Revised: November 20, 2023
Published online: December 15, 2023

[1] P. Cullinan, X. Muñoz, H. Suojalehto, R. Agius, S. Jindal, T. Sigsgaard, A. Blomberg, D. Charpin, I. Annesi-Maesano, M. Gulati, Y. Kim, A. L. Frank, M. Akgün, D. Fishwick, R. E. De La Hoz, S. Moitra, *Lancet Respir. Med.* **2017**, *5*, 445.
[2] a) International Agency for Research on Cancer, *"Silica, Some Silicates, Coal Dust, and Para-Aramid Fibrils"*, IARC Monographs on the Evaluation of Carcinogenic Risks to Humans, Vol. *68*, **1997**; b) International Agency for Research on Cancer, *"Arsenic, Metals, Fibres and Dusts"*, IARC Monographs on the Evaluation of Carcinogenic Risks to Humans, Vol. *100C*, **2012**; c) C. C. Leung, I. T. S. Yu, W. Chen, *Lancet* **2012**, *379*, 2008; d) K. M. Pollard, *Front. Immunol.* **2016**, *7*, 97; e) S. Harikrishnan, P. Jeemon, G. K. Mini, K. R. Thankappan, P. G. B. D Sylaja, *GBD 2017 Causes of Death Collaborators, Global, Regional, and National Age-Sex-Specific Mortality for 282 Causes of Death in 195 Countries and Territories, 1980–2017: a Systematic Analysis for the Global Burden of Disease Study 2017*, **2018**.
[3] a) K. Donaldson, *Ann. Occup. Hyg.* **1998**, *42*, 287; b) C. Pavan, B. Fubini, *Chem. Res. Toxicol.* **2017**, *30*, 469; c) E. T. Nij, D. Höhr, P. Borm, I. Burstyn, J. Spierings, F. Steffens, M. Lumens, T. Spee, D. Heederik, *J. Occup. Environ. Hyg.* **2004**, *1*, 191.
[4] a) V. Vallyathan, J. H. Kang, K. Van Dyke, N. S. Dalai, V. Castranova, *J. Toxicol. Environ. Health, Part A* **1991**, *33*, 303; b) J. Bruch, S. Rehn, B. Rehn, P. J. A. Borm, B. Fubini, *Int. J. Hyg. Environ. Health* **2004**, *207*, 203.
[5] a) E. Hnizdo, *Occup. Environ. Med.* **2003**, *60*, 237; b) A. M. Schrader, J. I. Monroe, R. Sheil, H. A. Dobbs, T. J. Keller, Y. Li, S. Jain, M. S. Shell, J. N. Israelachvili, S. Han, *Proc. Natl. Acad. Sci. U. S. A.* **2018**, *115*, 2890.

[6] F. Weinhold, R. West, *Organometallics* **2011**, *30*, 5815.
[7] a) C. R. Kurkjian, G. W. Kammlott, M. M. Chaudhri, *J. Am. Ceram. Soc.* **1995**, *78*, 737; b) P. L. Guzzo, F. B. Marinho De Barros, B. R. Soares, J. B. Santos, *Powder Technol.* **2020**, *368*, 149.
[8] a) G. Gorrasi, A. Sorrentino, *Green Chem.* **2015**, *17*, 2610; b) V. V. Boldyrev, K. Tkáčová, *J. Mater. Synth. Process.* **2000**, *8*, 121; c) P. B. Dempster, P. D. Ritchie, *Nature* **1952**, *169*, 538; d) G. Nagelschmidt, R. L. Gordon, O. G. Griffin, *Nature* **1952**, *169*, 539.
[9] T. Nash, A. C. Allison, J. S. Harington, *Nature* **1966**, *210*, 259.
[10] a) C. Pavan, R. Santalucia, R. Leinardi, M. Fabbiani, Y. Yakoub, F. Uwambayinema, P. Ugliengo, M. Tomatis, G. Martra, F. Turci, D. Lison, B. Fubini, *Proc. Natl. Acad. Sci. U. S. A.* **2020**, *117*, 27836; b) C. Pavan, M. J. Sydor, C. Bellomo, R. Leinardi, S. Cananà, R. L. Kendall, E. Rebba, M. Corno, P. Ugliengo, L. Mino, A. Holian, F. Turci, *Colloids Surf., B* **2022**, *217*, 112625; c) R. Leinardi, C. Pavan, H. Yedavally, M. Tomatis, A. Salvati, F. Turci, *Arch. Toxicol.* **2020**, *94*, 2981; d) C. Bellomo, C. Pavan, G. Fiore, G. Escolano-Casado, L. Mino, F. Turci, *Int. J. Mol. Sci.* **2022**, *23*, 15425.
[11] F. Turci, C. Pavan, R. Leinardi, M. Tomatis, L. Pastero, D. Garry, S. Anguissola, D. Lison, B. Fubini, *Part. Fibre Toxicol.* **2015**, *13*, 32.
[12] a) D. L. Griscom, *J. Non-Cryst. Solids* **1985**, *73*, 51; b) L. Skuja, *J. Non-Cryst. Solids* **1994**, *179*, 51; c) A. S. Zyubin, A. M. Mebel, S. H. Lin, Y. D. Glinka, *J. Chem. Phys.* **2002**, *116*, 9889.
[13] a) L. Skuja, H. Hosono, M. Hirano, in, *Laser-Induced Damage in Optical Materials: 2000* (Eds: G. J. Exarhos, A. H. Guenther, M. R. Kozlowski, K. L. Lewis, M. J. Soileau), Vol. *4347*, SPIE, Boulder, CO **2001**; b) A. Corazza, B. Crivelli, M. Martini, G. Spinolo, A. Vedda, *Phys. Rev. B* **1996**, *53*, 9739; c) J. Götze, M. Plötze, D. Habermann, *Mineral. Petrol.* **2001**, *71*, 225.
[14] A. Rimola, D. Costa, M. Sodupe, J.-F. Lambert, P. Ugliengo, *Chem. Rev.* **2013**, *113*, 4216.
[15] a) J. Arends, A. Dekker, W. Perdok, *Phys. Status Solidi B* **1963**, *3*, 2275; b) B. Fubini, E. Giamello, L. Pugliese, M. Volante, *Solid State Ionics* **1989**, *32*, 334.
[16] V. Murashov, *J. Mol. Struct.* **2003**, *650*, 141.
[17] a) V. V. Murashov, E. Demchuk, *Surf. Sci.* **2005**, *595*, 6; b) V. V. Murashov, E. Demchuk, *J. Phys. Chem. B* **2005**, *109*, 10835; c) V. V. Murashov, *J. Phys. Chem. B* **2005**, *109*, 4144.
[18] F. Di Benedetto, A. Giaccherini, M. Romanelli, G. Montegrossi, E. Belluso, S. Capella, A. Zoleo, G. Arcangeli, A. Marinaccio, O. Gottardo, F. Capacci, *Phys. Chem. Miner.* **2021**, *48*, 9.
[19] a) N. S. Dalal, X. Shi, V. Vallyathan, *J. Toxicol. Environ. Health, Part A* **1990**, *29*, 307; b) B. Fubini, V. Bolis, A. Cavenago, M. Volante, *Scand. J. Work, Environ. Health* **1995**, *21*, 9.
[20] a) M. Hasegawa, M. Kimata, S.-I. Kobayashi, *J. Appl. Polym. Sci.* **2001**, *82*, 2849; b) M. Kimata, M. Hasegawa, N. Kotake, *Powder Technol.* **2013**, *235*, 336.
[21] a) M. Romanelli, F. Di Benedetto, G. Fornaciai, M. Innocenti, G. Montegrossi, L. A. Pardi, A. Zoleo, F. Capacci, *Phys. Chem. Miner.* **2015**, *42*, 363; b) K. Gobindlal, Z. Zujovic, P. Yadav, J. Sperry, C. C. Weber, *J. Phys. Chem. C* **2021**, *125*, 20877.
[22] a) A. Rimola, M. Fabbiani, M. Sodupe, P. Ugliengo, G. Martra, *ACS Catal.* **2018**, *8*, 4558; b) O. El Samrout, M. Fabbiani, G. Berlier, J.-F. Lambert, G. Martra, *Langmuir* **2022**, *38*, 15516.
[23] a) H. He, X. Wu, H. Xian, J. Zhu, Y. Yang, Y. Lv, Y. Li, K. O. Konhauser, *Nat. Commun.* **2021**, *12*, 6611; b) J. Stone, J. O. Edgar, J. A. Gould, J. Telling, *Nat. Commun.* **2022**, *13*, 4529; c) H. He, X. Wu, J. Zhu, M. Lin, Y. Lv, H. Xian, Y. Yang, X. Lin, S. Li, Y. Li, H. H. Teng, M. H. Thiemens, *Proc. Natl. Acad. Sci. U. S. A.* **2023**, *120*, 2221984120; d) X. Wu, J. Zhu, H. He, H. Xian, Y. Yang, L. Ma, X. Liang, X. Lin, S. Li, K. O. Konhauser, *Commun. Earth Environ.* **2023**, *4*, 132.
[24] a) J. G. Croissant, K. S. Butler, J. I. Zink, C. J. Brinker, *Nat. Rev. Mater.* **2020**, *5*, 886; b) H. Zhang, D. R. Dunphy, X. Jiang, H. Meng, B. Sun, D. Tarn, M. Xue, X. Wang, S. Lin, Z. Ji, R. Li, F. L. Garcia, J. Yang, M. L. Kirk, T. Xia, J. I. Zink, A. Nel, C. J. Brinker, *J. Am. Chem. Soc.* **2012**, *134*, 15790.
[25] Y. Xia, J. Li, Y. Zhang, Y. Yin, B. Chen, Y. Liang, G. Jiang, R. N. Zare, *Proc. Natl. Acad. Sci. U. S. A.* **2023**, *120*, 2302014120.
[26] G. Hochstrasser, J. F. Antonini, *Surf. Sci.* **1972**, *32*, 644.
[27] a) Tatsuro Fukuchi, *Appl. Radiat. Isot.* **1996**, *47*, 1509; b) T. Fukuchi, *Appl. Radiat. Isot.* **1993**, *44*, 179.
[28] V. A. Radtsig, A. V. Bystrikov, *Kinet. Katal.* **1978**, *19*, 713.
[29] a) D. L. Griscom, E. J. Friebele, *Phys. Rev. B* **1981**, *24*, 4896; b) A. H. Edwards, W. B. Fowler, *Phys. Rev. B* **1982**, *26*, 6649.
[30] D. L. Griscom, *J. Ceram. Soc. Jpn.* **1991**, *99*, 923.
[31] M. Stapelbroek, D. L. Griscom, E. J. Friebele, G. H. Sigel, *J. Non-Cryst. Solids* **1979**, *32*, 313.
[32] M. J. Nilges, Y. Pan, R. I. Mashkovtsev, *Phys. Chem. Miner.* **2008**, *35*, 103.
[33] a) F. Delogu, *J. Phys. Chem. C* **2011**, *115*, 21230; b) C. Damm, W. Peukert, *Langmuir* **2009**, *25*, 2264; c) D. A. Hendrix, S. T. Port, J. A. Hurowitz, M. A. Schoonen, *GeoHealth* **2019**, *3*, 28.
[34] a) G.-M. Rignanese, J.-C. Charlier, X. Gonze, *Phys. Chem. Chem. Phys.* **2004**, *6*, 1920; b) N. H. De Leeuw, F. M. Higgins, S. C. Parker, *J. Phys. Chem. B* **1999**, *103*, 1270.
[35] B. Fubini, E. Giamello, M. Volante, V. Bolis, *Toxicol. Ind. Health* **1990**, *6*, 571.
[36] C. Pavan, V. Rabolli, M. Tomatis, B. Fubini, D. Lison, *Part. Fibre Toxicol.* **2014**, *11*, 76.
[37] R. Leibe, S. Fritsch-Decker, F. Gussmann, A. M. Wagbo, P. Wadhwani, S. Diabaté, W. Wenzel, A. S. Ulrich, C. Weiss, *Small* **2023**, *19*, 2207593.
[38] R. P. Nolan, A. M. Langer, J. S. Harington, G. Oster, I. J. Selikoff, *Environ. Res.* **1981**, *26*, 503.
[39] a) S. Lu, R. Duffin, C. Poland, P. Daly, F. Murphy, E. Drost, W. Macnee, V. Stone, K. Donaldson, *Environ. Health Perspect.* **2009**, *117*, 241; b) W.-S. Cho, R. Duffin, M. Bradley, I. L. Megson, W. MacNee, J. K. Lee, J. Jeong, K. Donaldson, *Part. Fibre Toxicol.* **2013**, *10*, 55; c) C. Pavan, R. Santalucia, G. Escolano-Casado, P. Ugliengo, L. Mino, F. Turci, *Int. J. Mol. Sci.* **2023**, *24*, 11482.
[40] C. Antognelli, A. Gambelunghe, C. Del Buono, N. Murgia, V. N. Talesa, G. Muzi, *Chem.–Biol. Interact.* **2009**, *182*, 13.
[41] S. Stoll, A. Schweiger, *J. Magn. Reson.* **2006**, *178*, 42.
[42] R. Arienzo, E. Bresciano, *Rass. Med. Sper.* **1969**, *16*, 135.